Supporting Information

A hydrophobic ionic liquid enhances electrocatalytic hydrogen evolution reaction on high specific-surface ruthenium-doped cobalt catalysts

Tao Zhang [a], Longjiang Li [b,c,d] , Shucheng Liu[a], and Yi Liu *[a]

*E-mail: yliu9@gzu.edu.cn

[a]*School of Physical Sciences, Guizhou University, Guiyang 550025, China*

[b]*Mining College, Guizhou University, Guiyang 550025, China.*

[c]*National & Local Joint Laboratory of Engineering for Effective Utilization of Regional Mineral Resources from Karst Areas, Guiyang 550025, China.*

[d]*Guizhou Key Lab of Comprehensive Utilization of Nonmetallic Mineral Resources, Guiyang 550025, China.*

Experimental

Materials

Nafion perfluorinated resin solution (CAS: 31175-20-9, 5%) was purchased from Shanghai Titan Scientific Co., Ltd. Ruthenium(III) chloride trihydrate ($RuCl_3 \cdot 3H_2O$, CAS: 13815-94-6, 98%) , $[C_4mim]^+$ $[NTf_2]^-$ (CAS:174899-83-3, 99%) was purchased from Shanghai Titan Scientific Co., Ltd., Dilute sulfuric acid solution (H_2SO_4, CAS: 7664-93-9, 95.0~98.0%) was purchased from Chongqing Chuandong Chemical (Group) Co., Ltd. Methanol (CH_3OH, CAS: 67-65-1, 99.9%) and ethanol (CH_3CH_2OH, CAS: 64-17-5, specification: pharmaceutical grade, 99.5%) were purchased from Aladdin (Shanghai) Chemical Co., Ltd. Hexahydrate of cobalt(II) nitrate ($Co(NO_3)_2 \cdot 6H_2O$, CAS: 10026-22-9, 99%) was purchased from Adamas-beta (Shanghai) Chemical Reagent Co., Ltd. 2-Methylimidazole ($C_4H_6N_2$, CAS: 693-98-1, 98%) was purchased from Sigma-Aldrich (Shanghai) Trading Co., Ltd. All chemicals and materials were utilized without further purification.

Synthesis

1. Preparation of metal-organic framework ZIF-67

1.455 g (0.5 mmol) of cobalt nitrate hexahydrate ($Co(NO_3)_2 \cdot 6H_2O$) and 1.642 g (2 mmol) of 2-methylimidazole ($C_4H_6N_2$, 2-methylimidazole) were separately dissolved

in 40 mL of methanol (CH_3OH) and 40 mL of anhydrous ethanol (CH_3CH_2OH). Each solution was stirred for 30 minutes.The mixture of $Co(NO_3)_2 \cdot 6H_2O$ in methanol was added dropwise to the mixture of 2-methylimidazole in ethanol. The resulting mixture was then stirred magnetically at room temperature for 24 hours. The precipitate was collected by centrifugation and washed several times with ethanol. The obtained purple powder was dried in an oven at 80°C for 10 hours and labeled as ZIF-67.

2. Preparation of Ru-loaded ZIF-67

Ruthenium loading was performed using a ball milling method. 50 mg $RuCl_3 \cdot 3H_2O$ were mixed with 1000 mg ZIF-67 powder through wet ball milling. Ethanol solution was added as a mixing medium during ball milling. The ball milling process was carried out in a planetary ball mill (parameters: 400 r min^{-1}, 10 min with direction change every time, total milling time 240 min). The resulting mixture was then retrieved, dried, and labeled as Ru@ZIF-67.

3. Preparation of Ru-Co/C Composite

The obtained Ru@ZIF-67 powder was subjected to high-temperature carbonization under an inert gas atmosphere (Ar, the gas flow rate is 60 L min^{-1}). The tube furnace heating conditions were set as follows: reaching a maximum temperature of 600 °C, maintaining this temperature for 120 minutes, with a heating rate of 3 °C min^{-1}. After cooling, the material was retrieved and designated as Ru-Co/C.

4. Modification of Ru-Co/C with ionic liquid ($[C_4mim]^+ [NTf_2]^-$)

Prepare several batches, each consisting of 10 mg of Ru-Co/C. Subsequently, add 10 μL, 30 μL, 50 μL, and 70 μL of ionic liquid (IL), respectively, along with 490 μL, 470 μL, 450 μL, and 430 μL of isopropanol to dilute and disperse the mixtures. After that, sonicate the mixtures for 90 minutes. Dry the sonicated mixtures in a vacuum drying oven at 50 °C under high vacuum conditions for at least 48 hours. Once the IL on the surface of the samples has completely evaporated, remove the samples and add 30 μL of Nafion and 470 μL of ethanol, followed by 60 minutes of sonication to prepare the catalyst ink.

Materials characterization

X-ray diffraction (XRD) were performed in a Bruker D8 Advance model X-ray diffractometer measurement with $Co_{K\alpha}$ radiations. TEM were performed in a High-resolution transmission electron microscope (HR-TEM) (FEl Tecnai G2 F30). The inductively coupled plasma optical emission spectrometer (ICP-OES) was employed in Agilent720ES model ICP-OES measurement. Surface area measurement was conducted using a BET measurement instrument BSD-PS(M). In-situ X-ray photoelectron spectroscopy (XPS) measurement was performed on a ThermoFischer Escalab 250Xi device. Fourier Transform Infrared Spectroscopy (FTIR) measurement was performed on a Nicolet lS10 device. Contact angle test was conducted using a LAUDA SCientific device (LAS100).

Electrochemical measurements

Electrochemical performance was assessed on a CHI-760E workstation at room temperature. All tests were carried out in a 1M H_2SO_4 electrolyte using a conventional three-electrode configuration. The reference electrode employed is an Ag/AgCl electrode, the counter electrode is made of graphite, and the working electrode consists of catalyst-modified glassy carbon (GC). The catalyst ink comprises 10 mg of the catalyst and 30 μL of a 5 wt% Nafion solution, which is ultrasonically dispersed in 470 μL of anhydrous ethanol. Then 10 μL of the homogeneous dispersion was transferred onto the surface of the GC substrate (0.07065 cm^{-2}) and dried at room temperature. The catalyst mass loading was approximately 0.28 mg cm^{-2}_{disk}. Polarization curves were recorded using linear sweep voltammetry (LSV) with scan rate of 5 mV s^{-1}. Cyclic voltammetry (CV) curves were obtained in the potential window of 0 V – 0.1 V (vs. RHE) with different scan rate from 5 to 100 mV s^{-1} to calculate the electrochemical double-layer capacitance.

The electrode potential in acidic solutions can be converted to a potential relative to the reversible hydrogen electrode (RHE) using the following equation:

$$E(\text{vs. RHE}) = E(\text{vs. Ag/AgCl}) + 0.1970 + 0.0591 \times \text{pH}$$

Molecular Dynamics Calculations

Molecular dynamics (MD) simulations were conducted using the Forcite module

within the Materials Studio software suite. The chemical structure of the Nafion membrane, characterized by its variable side-chain length (x = 6–10), is depicted in Fig.S8. The equivalent weight (EW), defined as the mass of the polymer per mole of sulfonic acid groups, serves as a critical parameter for membrane performance. Among the various Nafion membranes, Nafion 117 (EW = 1100 g, x≈6.54) has been extensively utilized in experimental studies and is widely regarded as a benchmark for the development of next-generation polymer electrolytes. Consequently, this study focuses primarily on Nafion 117, adopting x = 7 and n = 10 as representative structural parameters.

Five distinct aqueous systems were constructed, each comprising 2000 H_2O molecules, 100 H_3O^+ ions, and 10 Nafion 117 chains. The ionic liquid (IL) concentration was systematically varied across the models, with 0, 50, 100, 300, and 500 IL molecules incorporated (hereafter referred to as 0 IL, 50 IL, 100 IL, 300 IL, and 500 IL for clarity). To ensure conformational stability, system chirality, and equilibrium density, NPT ensemble equilibration was performed at 298 K and 0.0001 GPa, with each simulation running for 500 ps using a 1 fs timestep. Following equilibration, production runs were conducted under the NVT ensemble to generate metastable configurations, maintaining identical temperature and pressure conditions while extending the simulation duration to 1000 ps.

Energy calculations were performed using the COMPASSIII force field (version 1.0). Charge interactions were evaluated through two distinct methods, yielding key metrics such as interaction energy per Å², hydrogen bond population, and geometric parameters (bond lengths and angles). Electrostatic interactions were computed via atom-based summation with cubic spline truncation (cutoff distance = 9.5 Å, spline width = 1 Å, buffer width = 0.5 Å). Van der Waals interactions were treated similarly, with long-range corrections applied. Hydrogen bond distributions were analyzed using the Ewald summation method, achieving an accuracy of 0.01 kcal/mol, with van der Waals interactions truncated at 9.5 Å and long-range corrections enabled.

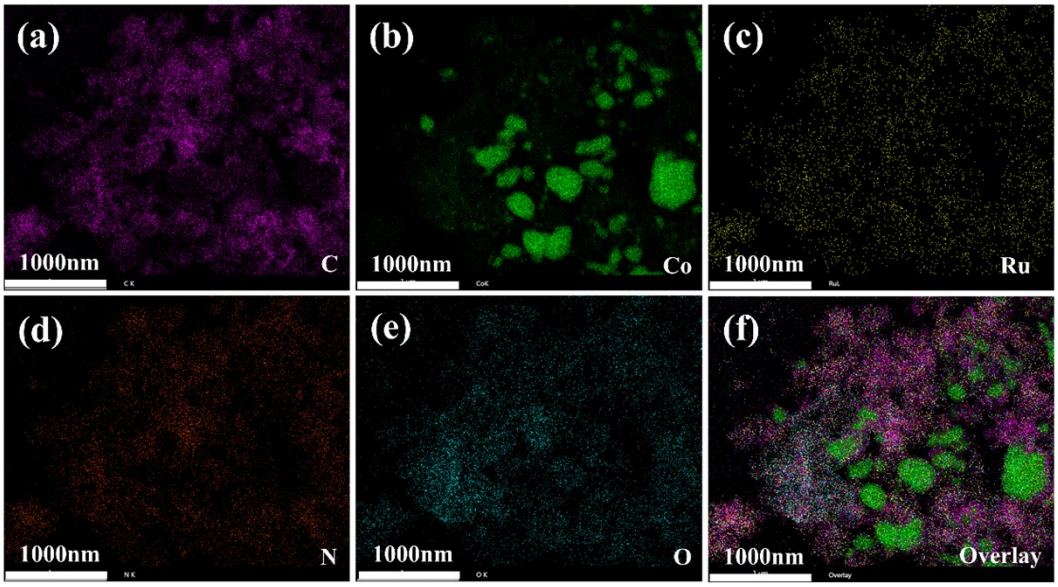

Fig. S1 HRTEM-EDX mapping of C, Co, Ru, N and O in Ru-Co/C.

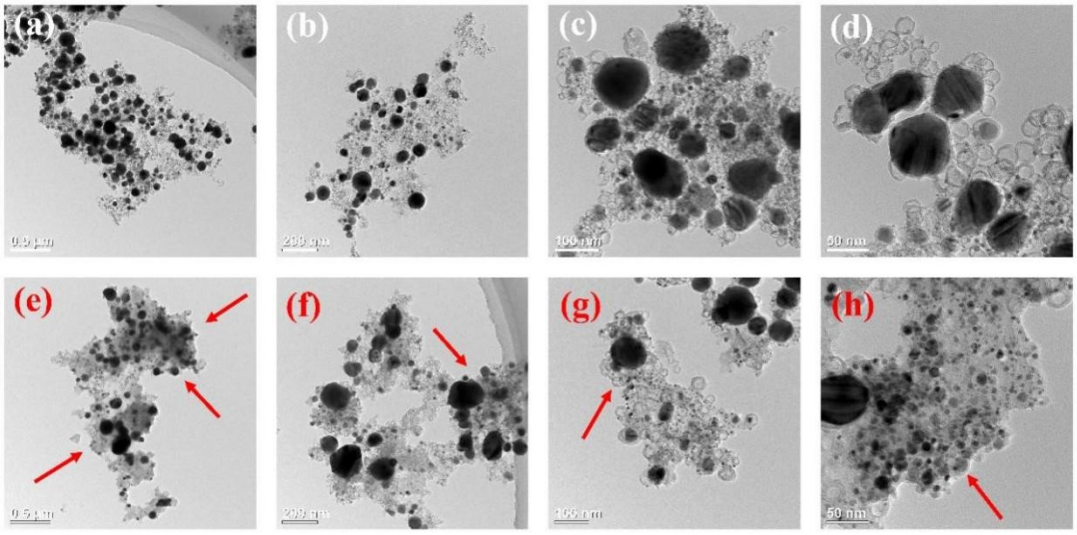

Fig. S2 (a), (b), (c) and (d) HRTEM images of Ru-Co/C. (e), (f), (g) and (h) HRTEM images of 30-IL-Ru-Co/C, with arrows indicating the agglomeration of ionic liquid.

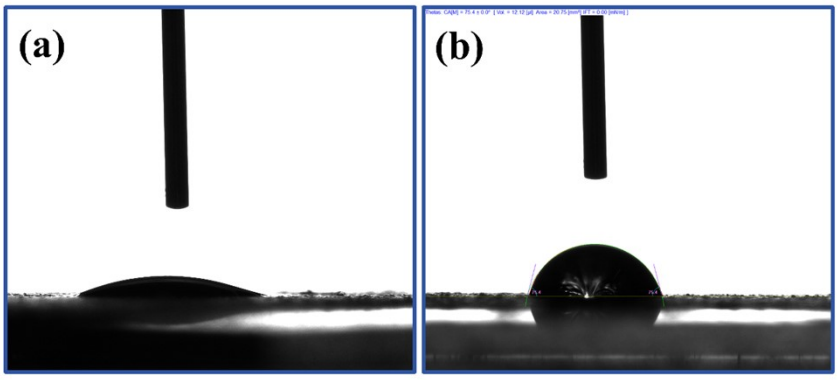

Fig S3. Contact angle test of (a)Ru-Co/C and (b) 30-IL-Ru-Co/C with water.

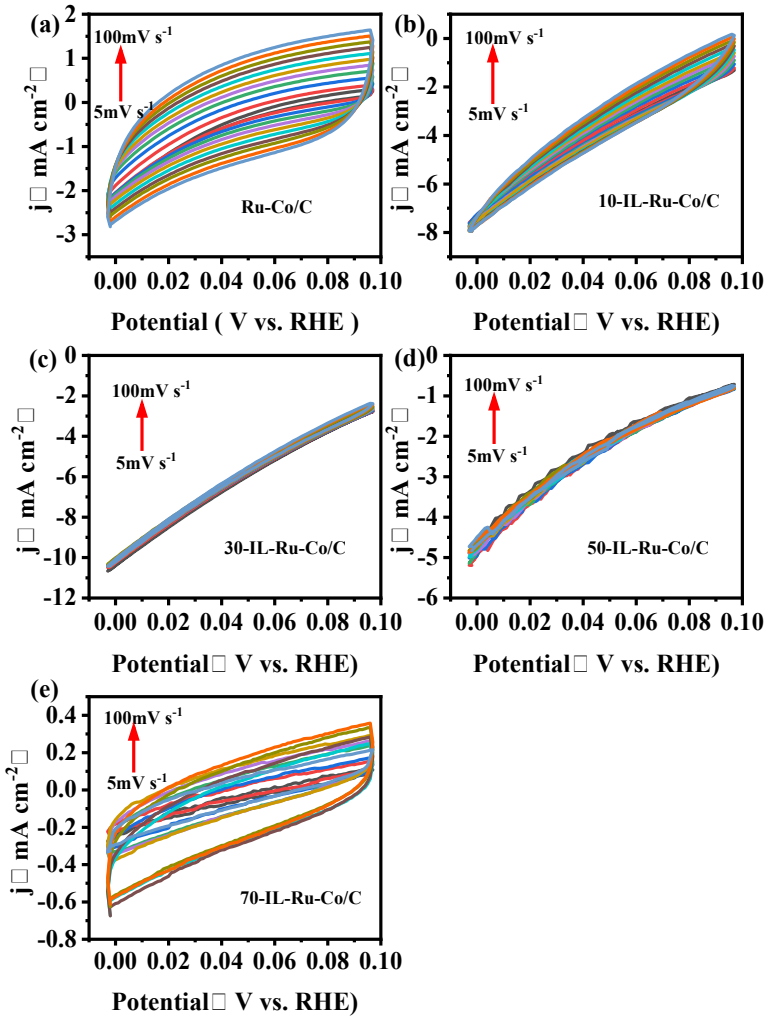

Fig. S4 Cyclic voltammetry (CV) curves in 1 M H_2SO_4 at different scan rates (5 mV s^{-1} to 100 mV s^{-1}) correspond to different concentrations of IL.

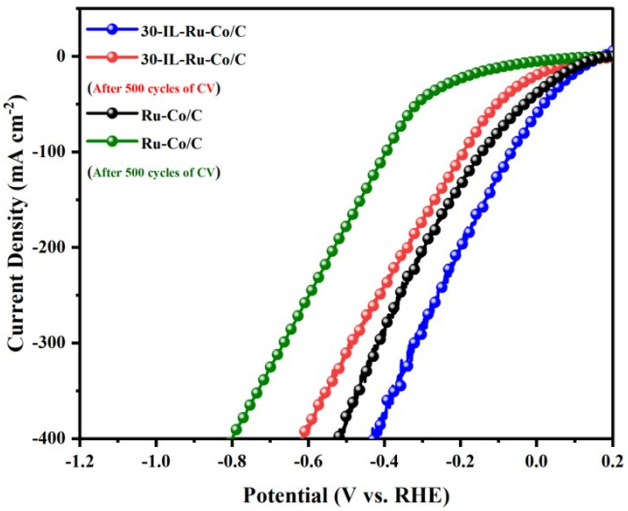

Fig. S5 LSV polarization curves of catalysts before and after 500 cycles of CV testing.

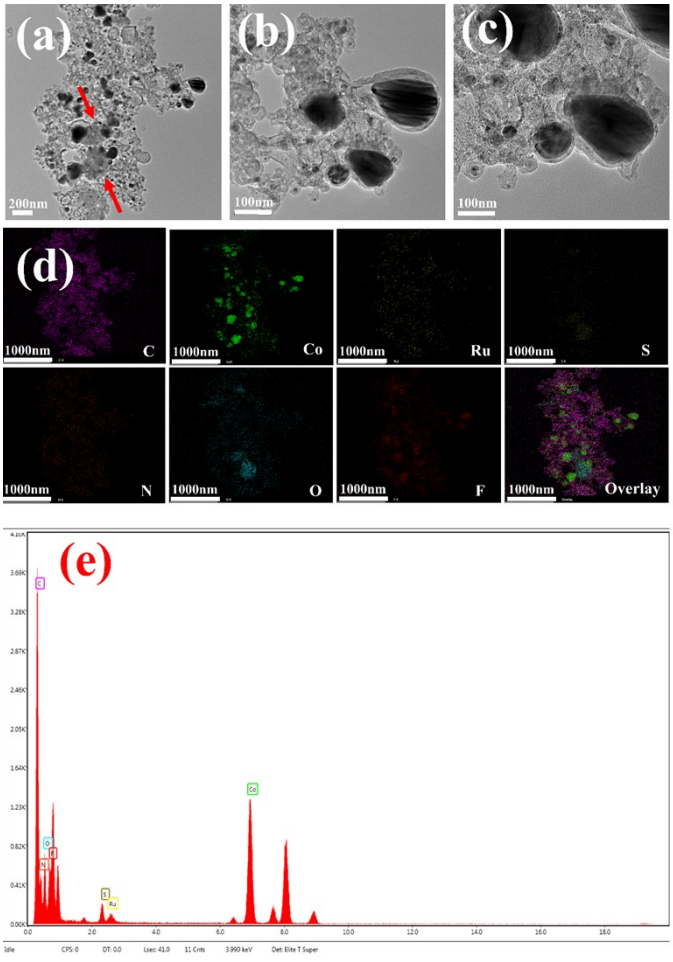

Fig. S6 (a)-(c) TEM images, (d) HRTEM-EDX mapping of C, Co, Ru, S, N, O, and F, (e) EDX energy spectrum of 30-IL-Ru-Co/C after undergoing 500 cycles of CV testing.

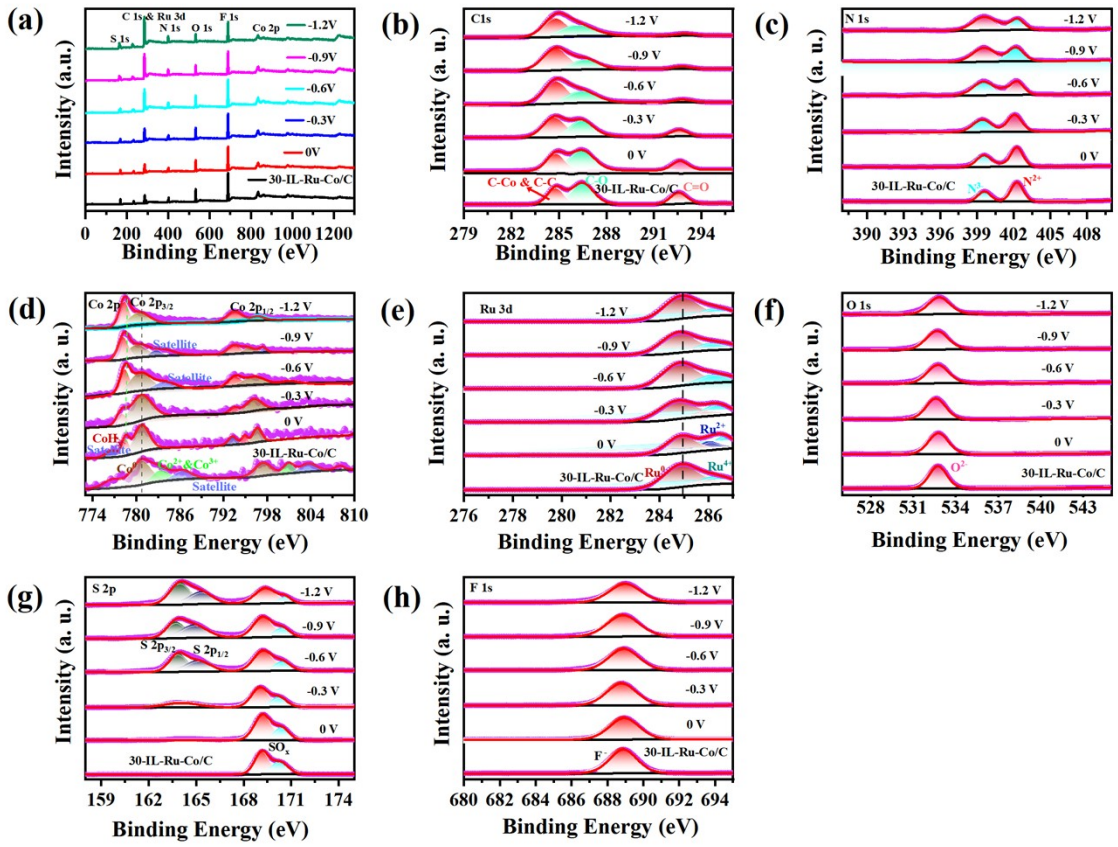

Fig. S7 In-situ XPS spectra of 30-IL-Ru-Co/C corresponding to increasing voltages under standard hydrogen electrode in 1M H_2SO_4. (a) XPS full spectrum, (b) C 1s , (c) N 1s , (d) Co 2p, (e) Ru 3d, (f) O 1s, (g) S 2p, (h) F 1s .

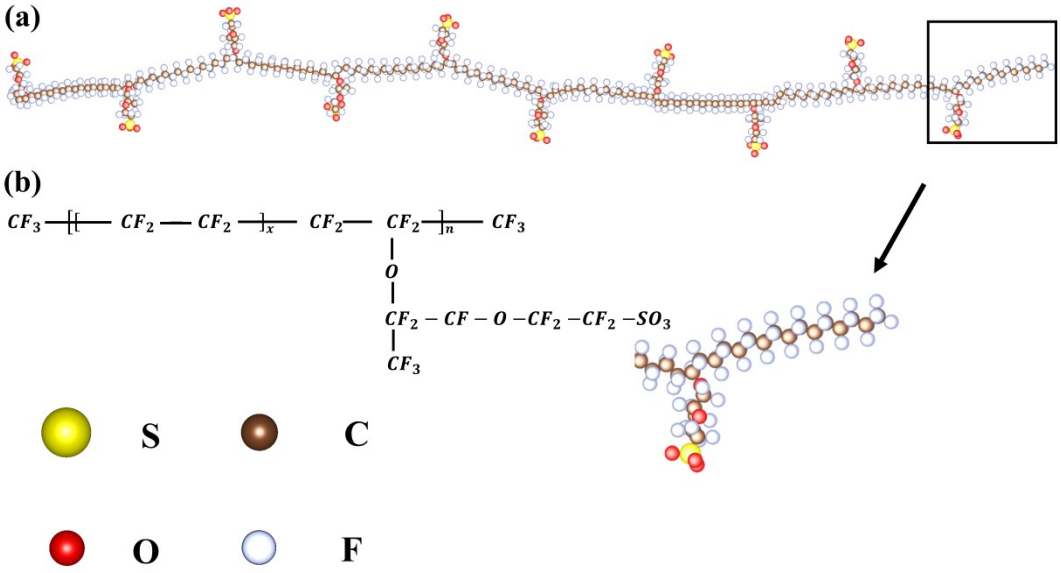

Fig. S8 The structure models of the Nafion membranes.

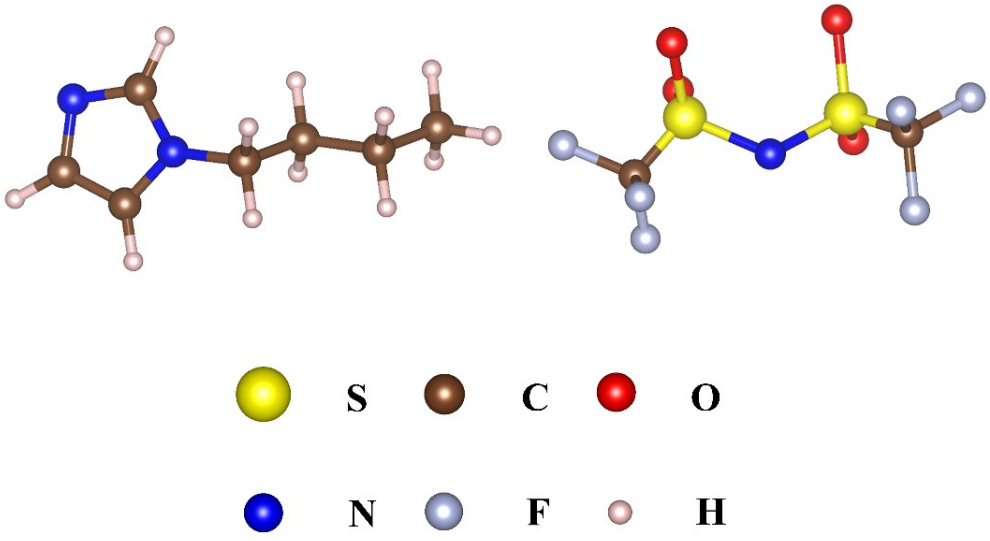

Fig. S9 The structure models of the IL $[C_4mim]^+[NTf_2]^-$ membranes.

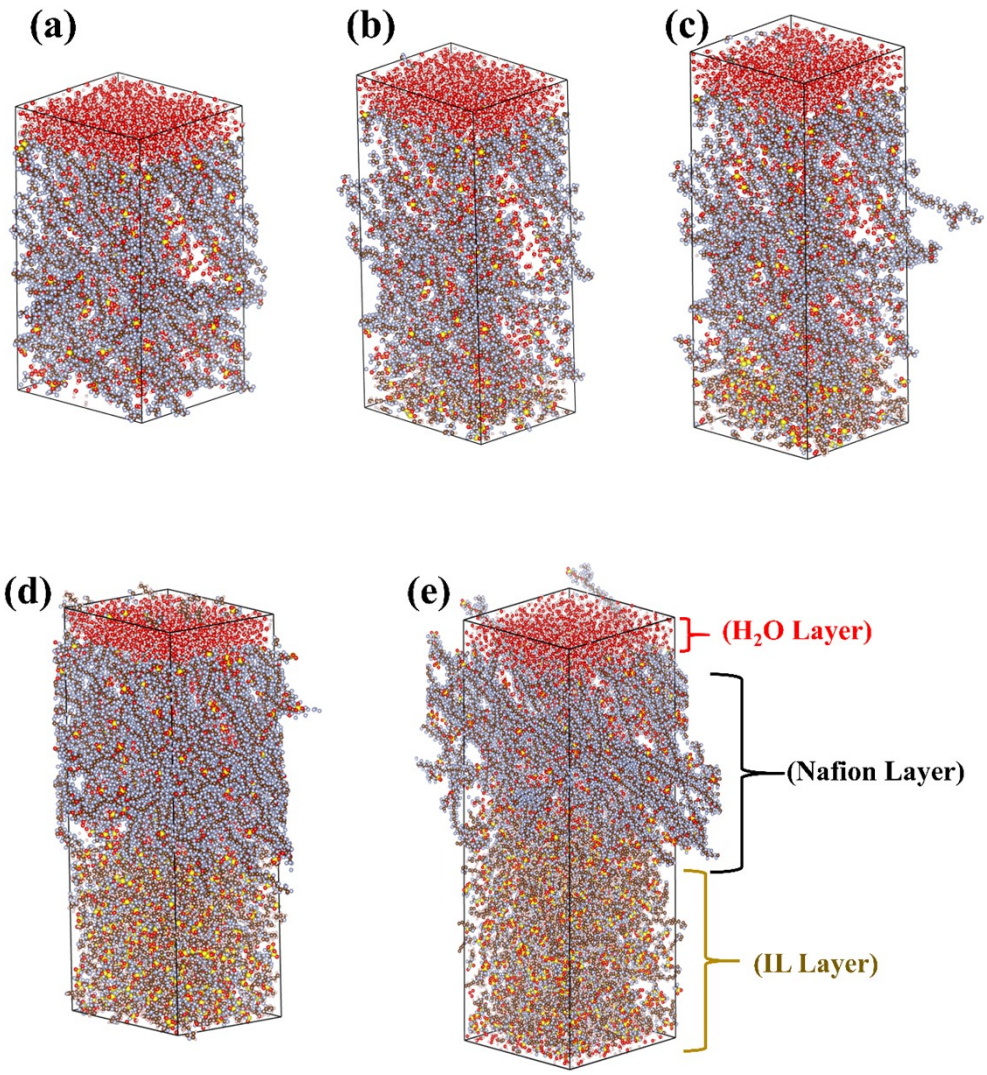

Fig. S10 The Water box of the (a) 0 IL, (b)50 IL, (c)100 IL, (d)300 IL and (e)500 IL, the layer between H_2O and Nafion is labeled as H_2O||Nafion layer, and similarly, the layer between IL and Nafion is labeled as IL||Nafion layer.

Table S1. The synthesis of Ru-Co/C was carried out using 1000 mg of ZIF-67 and 50 mg of $RuCl_3·3H_2O$ as precursors, followed by the addition of varying amounts of IL. The resultant Ru-Co/C samples were analyzed using ICP-OES.

	10-IL-Ru-Co/C	**30-IL-Ru-Co/C**	**50-IL-Ru-Co/C**	**70-IL- Ru-Co/C**
ZIF-67 (mg)	1000	1000	1000	1000
$RuCl_3·3H_2O$ (mg)	50	50	50	50
ICP-OES	**Test element**	**Content of element in the Ru-Co/C (mg/kg)**		**Element content in the Ru-Co/C**
	Co	493317.70		49.3318%
	Ru	9684.90		0.9685%
IL (uL)	10	30	50	70

Table S2. Comparative study of typical HER catalysts.

Materials	**Overpotential/mV**	**Tafel slope /(mV·dec^{-1})**	**Electrolyte**	**Ref.**
Pt-GA-2	34(η_{100})	33.2	0.5 M H_2SO_4	1
Pt/C/NF	41(η_{10})	55.7	1.0 M KOH	2
Nanocrystalline Ni_5P_4	23(η_{10})	33.0	1.0 M H_2SO_4	3
β-PdHene	20(η_{10})	37.8	0.5 M H_2SO_4	4
Ru-RuSi/C	27(η_{10})	27	1.0 M KOH	5
a-Ru-GNL_{500}	23(η_{10})	49	1.0 M KOH	6
Rh-WNO	22(η_{10})	34	1.0 M KOH	7
2.5%Ru-VS_2/CC	89(η_{10})	63	0.5 M H_2SO_4	8
ZIF-67@ZIF-8@Ru-900	13(η_{10})	40.6	1.0 M KOH	9
	29(η_{10})	41.8	0.5 M H_2SO_4	
S-RuO_2	25(η_{10})	32.6	1.0 M KOH + 3.5 wt % NaCl	10
Co−P3O/F-TiO_2	189(η_{100})	64.0	1.0 M KOH	11
Ni_2P/GCE	140(η_{20})	87.0	1.0 M H_2SO_4	12
CoP/GQDs/S−TiO_2	189(η_{100})	93	1 M KOH	13
SnS/$NiFe_2O_4$/NF	68 (η_{10})	115	1.0 M KOH	14

Ni@NC/Ru	28(η_{10})	42	1.0 M KOH	15
Ni_2P nanoparticle film/Ti	138(η_{20})	60.0	1.0 M H_2SO_4	16
poly[CoOTPc]+KB (3.5:1.5)	72(η_{10})	41	0.5 M H_2SO_4	17
SRO	28(η_{10})	29	0.5 M H_2SO_4	18
30-IL-Ru-Co/C	26(η_{20})	119.9	1.0 M H_2SO_4	This Work

Table S3. The table below summarizes the statistical data obtained from molecular dynamics simulations of the five water box models corresponding to 0 IL, 50 IL, 100 IL, 300 IL, and 500 IL.

Hydrogen-bond between Oxygen and Hydrogen atoms in water box model of 0 IL					
AverageNumBonds	2383	NumBondsMin	2277	NumBondsMax	2582
AverageLength	1.79	MinLength	1.18	MaxLength	2.20
AverageAngle	155.61	MinAngle	90.00	MaxAngle	179.97
Hydrogen-bond between Oxygen and Hydrogen atoms in water box model of 50 IL					
AverageNumBonds	2363	NumBondsMin	2203	NumBondsMax	2584
AverageLength	1.79	MinLength	1.14	MaxLength	2.20
AverageAngle	155.93	MinAngle	90.00	MaxAngle	179.99
Hydrogen-bond between Oxygen and Hydrogen atoms in water box model of 100 IL					
AverageNumBonds	2512	NumBondsMin	2253	NumBondsMax	2586
AverageLength	1.76	MinLength	1.02	MaxLength	2.20
AverageAngle	159.27	MinAngle	90.00	MaxAngle	179.94
Hydrogen-bond between Oxygen and Hydrogen atoms in water box model of 300 IL					
AverageNumBonds	2445	NumBondsMin	2111	NumBondsMax	2511
AverageLength	1.73	MinLength	1.11	MaxLength	2.10
AverageAngle	151.23	MinAngle	90.00	MaxAngle	179.95
Hydrogen-bond between Oxygen and Hydrogen atoms in water box model of 500 IL					
AverageNumBonds	2025	NumBondsMin	1826	NumBondsMax	2282
AverageLength	3.62	MinLength	2.86	MaxLength	4.00
AverageAngle	117.62	MinAngle	90.00	MaxAngle	179.83

Note: The analysis includes the relationship between the number of hydrogen-bond and the bond length between oxygen and hydrogen atoms, as well as the distribution of hydrogen-bond angles for each element, where “AverageNumBonds” represents the average number of hydrogen-bond calculated after each time step, “NumBondsMin” indicates the minimum number statistical analysis, “NumBondsMax” indicates the maximum number statistical analysis, “AverageLength” denotes the average bond length, “MinLength” refers to the minimum bond length, “MaxLength” refers to the maximum bond length, “AverageAngle” represents the average bond angle, “MinAngle” refers to the minimum bond angle, and “MaxAngle” refers to the maximum bond angle statistical analysis during the simulation.

References

1. H. Yao, X. Yu, Y.-X. Jia, J.-C. Zhang, J.-X. Yao, J.-Q. Liu, B.-L. Su and X.-H. Guo, *Rare Metals*, 2025, 1-9.

2. C. Lyu, C. Guan, K. Wu, Z. Wang, M. Sun, J. Yang, J. Cheng and Y. Liu, *Fuel*, 2025, **386**, 134285.

3. A. Laursen, K. Patraju, M. Whitaker, M. Retuerto, T. Sarkar, N. Yao, K. Ramanujachary, M. Greenblatt and G. Dismukes, *Energy & Environmental Science*, 2015, **8**, 1027-1034.

4. H. Wang, Y. Qin, Y. Wu, Y. Qiu, L. Ling, Q. Fang, C. Wang, L. Hu, W. Gu and C. Zhu, *Nature Communications*, 2024, **15**, 10289.

5. L. Hou, Z. Li, H. Jang, M. G. Kim, J. Cho, W. Zhong, s. Liu and X. Liu, *Angewandte Chemie*, 2024, e202423756.

6. G. M. Karim, A. Patra, S. K. Deb, H. Upadhya, S. Das, P. Mukherjee, W. Ahmad, N. Barman, R. Thapa and N. V. Dambhare, *Advanced Functional Materials*, 2024, 2315460.

7. B. Zhang, Y. Zheng, Z. Xing, Z. Wu, C. Cheng, T. Ma and S. Li, *Journal of Materials Chemistry A*, 2024, **12**, 4484-4491.

8. T. Wang, X. Zhang, X. Yu, Y. Liu, J. Li, Z. Liu, N. Zhao, J. Zhang, J. Niu and Q. Feng, *Nanoscale*, 2024, **16**, 11250-11261.

9. X. Huo, J. Huang, M. Gao, W. Zhu, W. Liu, Q. Liu, L. Cao, K. Kajiyoshi, Y. Zhao and Y. Liu, *ACS Applied Energy Materials*, 2024, **7**, 2862-2871.

10.Y. Liu, L. Wu, Y. Wang, L.-W. Shen, G. Tian, L. Cui, L. Qin, L. Zhou, Y. Zhang and F. Rosei, *ACS nano*, 2025.

11.S. Qian, T. Jiang, J. Wang, W. Yuan, D. Jia, N. Cheng, H. Xue, Z. Xu, R. Gautier and J. Tian, *ACS Catalysis*, 2024, **14**, 18690-18700.

12.L. Feng, H. Vrubel, M. Bensimon and X. Hu, *Physical Chemistry Chemical Physics*, 2014, **16**, 5917-5921.

13. J. Wang, S. Qian, D. Jia, Y. Zhang, H. Xue, T. Jiang, H. Zhang and J. Tian, *Inorganic Chemistry*, 2025.

14. G. John, V. G. Sree, M. Navaneethan and P. J. Jesuraj, *Applied Surface Science*, 2025, 162324.

15. Y. Yuan, J. Rong, L. Zheng, Z. Hu, S. Hu, C. Wu and Z. Zhuang, *International Journal of Hydrogen Energy*, 2024, **52**, 687-695.

16. Z. Pu, Q. Liu, C. Tang, A. M. Asiri and X. Sun, *Nanoscale*, 2014, **6**, 11031-11034.

17. N. Kousar and L. K. Sannegowda, *International Journal of Hydrogen Energy*, 2024, **50**, 37-47.

18. Y. Zhang, K. E. Arpino, Q. Yang, N. Kikugawa, D. A. Sokolov, C. W. Hicks, J. Liu, C. Felser and G. Li, *Nature Communications*, 2022, **13**, 7784.